THE JOURNAL OF BIOLOGICAL CHEMISTRY VOL. 284, NO. 26, pp. 17512–17520, June 26, 2009

mRNA Display Design of Fibronectin-based Intrabodies That Detect and Inhibit Severe Acute Respiratory Syndrome Coronavirus Nucleocapsid Protein*[S]

Received for publication, March 6, 2009 Published, JBC Papers in Press, April 13, 2009, DOI 10.1074/jbc.M901547200

Hsiang-I. Liao[‡1], C. Anders Olson[§1], Seungmin Hwang[‡], Hongyu Deng[‡], Elaine Wong[‡], Ralph S. Baric[¶], Richard W. Roberts[‖], and Ren Sun[‡2]**

*From the [‡]Department of Molecular and Medical Pharmacology and the **California Nano System Institute, UCLA, Los Angeles, California 90095, [§]Biochemistry and Molecular Biophysics Option, California Institute of Technology, Pasadena, California 91125, the [¶]Department of Epidemiology, University of North Carolina, Chapel Hill, North Carolina 27599, and the [‖]Department of Chemistry, Chemical Engineering, and Biology, University of Southern California, Los Angeles, California 90089-1211*

The nucleocapsid (N) protein of severe acute respiratory syndrome (SARS) coronavirus plays important roles in both viral replication and modulation of host cell processes. New ligands that target the N protein may thus provide tools to track the protein inside cells, detect interaction hot spots on the protein surface, and discover sites that could be used to develop new anti-SARS therapies. Using mRNA display selection and directed evolution, we designed novel antibody-like protein affinity reagents that target SARS N protein with high affinity and selectivity. Our libraries were based on an 88-residue variant of the 10th fibronectin type III domain from human fibronectin (10Fn3). This selection resulted in eight independent 10Fn3 intrabodies, two that require the N-terminal domain for binding and six that recognize the C terminus, one with K_d = 1.7 nM. 10Fn3 intrabodies are well expressed in mammalian cells and are relocalized by N in SARS-infected cells. Seven of the selected intrabodies tested do not perturb cellular function when expressed singly *in vivo* and inhibit virus replication from 11- to 5900-fold when expressed in cells prior to infection. Targeting two sites on SARS-N simultaneously using two distinct 10Fn3s results in synergistic inhibition of virus replication.

The ability to detect and inhibit protein function is central to molecular and cellular biology research. To date, phage display and monoclonal antibody production have been the most common routes to design reagents for protein detection and inhibition, antibodies and antibody-like reagents that serve as high affinity, high specificity molecular recognition tools (1). Totally *in vitro* selection methods using alternative scaffolds are becoming more common to produce affinity reagents with improved and expanded functionality (2, 3). For example, ribosome display and mRNA display enable creating 1–100 trillion-member peptide and protein libraries that surpass immunological and phage display diversities by 3–5 orders of magnitude (4).

Antibodies or antibody-like molecules are important because they can serve as diagnostics, probes for studying proteins *in vivo*, and potential therapeutics (or surrogate ligands for therapeutic design/screening). Regarding biology, antibodies used inside living cells, denoted "intrabodies," are appealing because they provide an alternative to genetic knock-outs, dominant negative mutations, and RNA interference strategies, enabling targeting proteins in a domain-, conformation-, and modification-specific fashion as well as identifying hot spots for protein interaction (5, 6). For example, green fluorescent protein-labeled intrabodies can act as molecular beacons to determine real time, live cell localization of endogenous target proteins rather than non-native expression of green fluorescent protein target fusions (7).

Although antibodies often demonstrate laudable affinity and selectivity, these proteins are likely to be suboptimal as a general approach to create intracellular reagents. Most notably, antibodies contain disulfide bonds that are likely to be reduced in the cytosol, thus impeding their proper folding and function (8). To overcome the paucity of functional intrabodies generated by *in vitro* selection methods, *in vivo* screens may be employed at the expense of combinatorial diversity (9). On the other hand, it has been demonstrated that intracellular antibodies can generate aggresomes, which may inhibit the ubiquitin-mediated degradation pathway and promote apoptosis (10–12).

Ideally, intrabodies would be as follows: 1) easy to produce in a broad variety of cells; 2) stable; 3) specific; 4) high affinity; 5) highly selective; 6) functional in intracellular environments; and 7) noninterfering with normal cellular processes. Recently, ribosome display has been used to generate protein affinity reagents based on ankyrin domains (DARPins), which detect and inhibit kinase or proteinase function *in vivo* (13, 14). Although this scaffold is powerful, it is structurally very different from antibodies as it utilizes a discontinuous binding surface rather than the continuous surface generated by the CDR loops in antibody V_H and V_L domains.

Our approach here has been to use mRNA display to design disulfide-free antibody-like proteins that can be used to create general protein targeting tools. To do this, we used a protein

* This work was supported, in whole or in part, by National Institutes of Health Grant RO1 GM60416 (to R. W. R.). This work was also supported by a microbial pathogenesis training grant from Burroughs Wellcome Fund.
[S] The on-line version of this article (available at http://www.jbc.org) contains supplemental Methods, additional references, and Figs. S1–S7.
[1] Both authors contributed equally to this work.
[2] To whom correspondence should be addressed: 650 Charles E. Young Dr. South, CHS 23-120, UCLA, Los Angeles, CA 90095. Fax: 310-825-6267; E-mail: rsun@mednet.ucla.edu.

library based on the 10th fibronectin type III domain of human fibronectin (10Fn3)[3] (15, 16). The 10Fn3 domain was developed as an antibody mimetic by Koide *et al.* (16) because of the following: 1) it is topologically analogous to the immunoglobulin V_H domain; 2) it is exceptionally stable; 3) it presents a continuous protein interaction surface; and 4) it expresses well in both eukaryotic and bacterial cells (16). We recently described construction and characterization of a 3×10^{13} member 10Fn3 library (15) and validated this library by developing proteins and fluorescence resonance energy transfer sensors that recognize IκBα in a phosphoserine-specific fashion (17). There the selected 10Fn3 functioned *in vivo*, blocking proteasome-mediated degradation of full-length IκBα efficiently.

Here we have targeted the severe acute respiratory syndrome (SARS-CoV) nucleocapsid protein (N). SARS-CoV is a unique member of the Coronaviridae family with only 20% sequence identity to the closest homolog (18). There is a need for reagents and methods that can be used to detect new infectious entities as they arise. Indeed, the recent SARS epidemic was unexpected, reaching an 8% fatality rate despite the fact that coronaviruses typically are involved in ~30% of common cold infections. N protein is 422 amino acids long, phosphorylated, and composed of two structured domains linked by a nonstructured domain. The N-terminal domain (NTD) is a putative RNA binding domain, and the C-terminal domain (CTD) mediates self-association (Fig. 1*A*) (19, 20). The unstructured middle domain interacts with the membrane (M) protein, anchoring M protein to the viral core. The two structured domains act in concert to bind genomic RNA, oligomerize, and form the final packaged ribonucleoprotein complex.

We chose N as our target for several reasons. First, the N protein is the most abundant protein produced by SARS virus. Second, N plays multiple roles *in vivo*, including binding/packaging the viral genomic RNA, mediating interactions with the viral membrane (via the M protein), acting in genome replication, and exerting control over host cell processes (21, 22). Finally, no therapeutic reagents currently target N protein; therefore, new inhibitory N-directed ligands represent an important potential new route for developing anti-SARS drugs.

After six rounds of selection, we were able to generate molecules that detect SARS N protein *in vitro* and modulate its SARS replication *in vivo* in a domain-specific manner. The selection yielded six high affinity molecules that recognize the CTD and two molecules that require the NTD for binding. We confirmed the interaction between the selected 10Fn3 proteins and N protein both *in vitro* and *in vivo* by pulldown, co-immunoprecipitation, and immunofluorescence microscopy. Seven of the 10Fn3-based intrabodies inhibit replication, ranging from 11- to 5900-fold, recognizing at least two nonoverlapping epitopes/hot spots in a synergistic manner. These molecules represent new tools for detecting SARS virus, assessing N function in living cells, and identifying regions of N critical for virus proliferation.

[3] The abbreviations used are: 10Fn3, human fibronectin 10th fibronectin type III domain; SARS-CoV, severe acute respiratory disorder coronavirus; N, nucleocapsid protein; s2m, stem-loop 2 motif; NTD, N-terminal domain; CTD, C-terminal domain; Ni-NTA, nickel-nitrilotriacetic acid; WT, wild type.

EXPERIMENTAL PROCEDURES

Cell Culture and Virus—293T, 293T-ACE2, and VERO cells were cultured in Dulbecco's modified Eagle's medium containing 10% fetal bovine serum and 1% penicillin/streptomycin. The 293-ACE2 is a stable cell line derived from 293T after co-transfecting ACE2 and a puromycin resistance plasmid. Wild type SARS-CoV Urbani strain was obtained from the Centers for Disease Control and Prevention. Both WT SARS-CoV and SARS-CoV *Renilla* luciferase recombinant virus were propagated in VERO cells (23, 24). The murine γ-herpesvirus 68-luciferase virus (MHV-68/M3FL) was constructed by inserting viral M3 promoter-driven firefly luciferase cassette between genomic coordinates 746 and 747 of MHV-68 (U97553).

Plasmids—SARS-CoV N protein was cloned from the cDNA derived from SARS-CoV-infected cell into bacteria expression plasmid pDW363C (25). N containing the biotinylation signal peptide tag was then subcloned into pcDNA3 (Invitrogen) for mammalian expression with a His tag. pTAG-N was constructed for mammalian expression of N protein with N-terminal FLAG and calmodulin-binding protein tag. N-ΔNTD and N-CTD were subcloned from pcDNA3-N by PCR. The selected 10Fn3 pool 6 cDNA was cloned into pCR4-TOPO using a TOPO TA cloning kit (Invitrogen). Selected molecules were further subcloned into pET11 (Novagen) for bacterial expression with C-terminal His_6 tag and pIRES-puro (Clontech) for mammalian expression with C-terminal FLAG tag.

Protein Purification—The N protein target was expressed and purified from transfected 293T cells using Lipofectamine Plus (Invitrogen). Cells were lysed using modified RIPA buffer (10 mM Tris, pH 8.0, 1% Nonidet P-40, 150 mM NaCl, 1 mM EDTA) and purified with Ni^{2+}-NTA beads. N protein was biotinylated *in vitro* using biotin ligase (Avidity) and conjugated to streptavidin acrylamide or neutravidin-agarose beads (Pierce). Selected 10Fn3 proteins were expressed using *Escherichia coli* BL-21 (DE3) cultures induced at OD ~0.4 with 1 mM isopropyl 1-thio-β-D-galactopyranoside for 3 h at 37 °C. The proteins were purified with Ni^{2+}-NTA beads (Qiagen).

mRNA Display—For the first round of selection, a library of approximately 1 trillion unique DNA molecules was amplified by PCR. For each round of selection, the PCR product was transcribed by *in vitro* runoff transcription with T7 RNA polymerase. Library RNA was ligated with T4 DNA ligase (PerkinElmer Life Sciences) to a DNA linker that contains puromycin at the 3′ end (pF30P, 5′-phospho-A_{21}-9_3-ACC-Pu, where 9 is phosphoramidite spacer 9, and Pu is puromycin, Glen Research Corp.). Ligation was mediated by a splint complementary to the 3′ library and 5′ linker sequences (Fn-pF30P-Splint, 5′-TTTT-TTTTTTTTGGAGCCGCTACC). Ligated library mRNA was purified by urea-PAGE and translated *in vitro* with rabbit reticulocyte lysate (Red NOVA, Novagen). Fusion formation was enhanced by addition of potassium and magnesium as described previously (26). RNA-10Fn3 fusions were purified by binding at 4 °C to oligo(dT)-cellulose beads (PerkinElmer Life Sciences) in oligo(dT) isolation buffer (100 mM Tris, pH 8, 1 M NaCl, 0.2% Triton X-100), eluted in 10 mM Tris, pH 8, at room temperature, and desalted (Nap-25, GE Healthcare or Centrisep, Princeton Separations). The fusions were reverse-tran-

scribed (Superscript II, Invitrogen) prior to affinity enrichment with immobilized N protein. Binding and washing buffer contained 1× TBS (20 mM Tris, pH 8, 150 mM NaCl) plus 0.02% Tween 20, 0.5 mg/ml bovine serum albumin (Sigma), and 0.1 mg/ml sheared salmon sperm DNA (Sigma). After round one, fusion pools were subjected to FLAG tag purification with anti-FLAG M2-agarose beads (Sigma) and were eluted with 3× FLAG peptide (Sigma). Rounds 2–6 also included a preclearing step to remove background binders using empty beads prior to the selection. Binding and washing were performed at 4 °C for rounds 1–5 and at 37 °C for round 6.

In Vitro Binding Assay—For 10Fn3 pools, radiolabeled fusions were prepared as described for the selection, except the translations were supplemented with L-[^{35}S]methionine (MP Biomedicals). Fusion pools were incubated with ribonuclease A (Roche Applied Science) prior to measuring binding efficiencies. Individual pool 6 clones were amplified from pCR4-TOPO. Following *in vitro* transcription, the purified unique 10Fn3 RNA products were translated *in vitro* with rabbit reticulocyte lysate (Red Nova, Novagen) in the presence of L-[^{35}S]methionine. Translated 10Fn3 proteins were then FLAG tag-purified with anti-FLAG M2-agarose beads (Sigma) using 3× FLAG peptide for elution. Radiolabeled 10Fn3 pools and individual pool 6 N-binding 10Fn3 proteins were incubated with immobilized N protein or empty beads. After washing in selection buffer, binding efficiencies were determined by scintillation counting. Pool binding assays were performed at either 4 or 37 °C, as indicated. Individual clone bindings were performed at room temperature.

Pulldown and Co-immunoprecipitation Assays—Purified 10Fn3 proteins immobilized on Ni^{2+}-NTA-agarose beads were used to pull down recombinant p-TAG-N protein from crude 293T cell lysate overnight at 4 °C. For co-immunoprecipitation, 293T cells were co-transfected with plasmids bearing His-tagged N and FLAG-tagged 10Fn3 proteins. The harvested cell lysate was incubated overnight at 4 °C with protein G-Sepharose beads (Amersham Biosciences) conjugated with either the anti-FLAG antibody (Sigma) to precipitate 10Fn3 proteins or anti-mouse IgG as negative control. For domain mapping by pulldown, the mammalian N-WT, N-ΔNTD, and N-CTD were immobilized on Ni-NTA beads and were used to pull down 10Fn3 proteins bearing a FLAG tag from transfected 293T cell lysate overnight in 4 °C. The co-immunoprecipitation and pulldown assays were performed with modified RIPA buffer and analyzed by Western blots.

Surface Plasmon Resonance—Binding kinetics were measured by a Biacore T100 instrument using a streptavidin sensor chip. N protein purified from 293T cells was loaded at a density of 800 response units. Various concentrations of either Fn-N17 or Fn-N22 purified from *E. coli* BL21(DE3) were flowed over a blank streptavidin chip and the N bound chip at 100 μl/min for 120 s and were allowed to fall off for 1 h. Kinetic data were obtained by fitting with Biacore evaluation software.

Immunofluorescence Microscopy—VERO cells were transfected in 8-well chamber slides with 10Fn3 intrabodies and infected with SARS-CoV. Infected and noninfected cells were fixed with 2% paraformaldehyde. The immunofluorescence was done following the standard protocol. 10Fn3 intrabodies were detected by anti-FLAG antibody (Sigma) and Alexa Fluor 488 goat anti-mouse IgG (Invitrogen). The N proteins were detected by polyclonal anti-SARS N protein antibody (Imgenex) and goat anti-rabbit Cy3-conjugated antibody (Invitrogen).

SARS-CoV Inhibition Assay—293T cells were transfected with 10Fn3 intrabodies or empty plasmid and infected with SARS-CoV *Renilla* luciferase as described. *Renilla* luciferase was used as a reporter to correlate the virus titer of transfected cell supernatants. Supernatants were collected from transfected cells 20 h post-infection and used to infect fresh 293T-ACE2 cells (secondary reporter cells). The secondary reporter cells were collected at 16 h post-infection and assayed for luciferase activity. Primary transfected cells were harvested after supernatant transfer to determine relative protein expression. All cells were collected with Passive Lysis Buffer for analysis by *Renilla* luciferase assay system (Promega).

Real Time Quantitative PCR—Total RNAs were extracted from the SARS-CoV-infected cells first by TRI Reagent (Invitrogen), and then 10 μg of the total RNA were purified by micro-to-midi RNA purification system (Invitrogen). The cDNAs were made from reverse transcription of 1 μg of purified RNA using random hexamers and Superscript III (Invitrogen). Viral N gene transcripts were amplified by primers SARS/qPCR-NF and SARS/qPCR-NR, following the standard SYBR green quantitative PCR protocol. Standards for copy number calculation were derived from cloning amplified PCR product. Quantitative PCR for human β-actin was done as a normalization control using primers ACTB-5F and ACTB-3R.

RNA Band Shift—A 32-mer RNA composing the stem loop 2 motif was created using runoff transcription (27). The T7 promoter oligonucleotide (5′-TCCTAATACGACTCACTATAG) was annealed to the template oligonucleotide (5′-CTGTACC-CTCGATCGTACTCCGCGTGGCCTCGCCTATAGTGAG-TCGTATTAGGA) and added (500 nM) to transcription buffer (80 mM HEPES, pH 7.5, 2 mM spermidine, 20 mM dithiothreitol, 25 mM $MgCl_2$ supplemented with 4 mM NTPs). Transcription was carried out at 37 °C for 2 h. After addition of excess EDTA, the sample was phenol/chloroform-extracted and purified by denaturing urea-PAGE. N protein was purified as described above and treated with DNase I and RNase A. The N protein sample was then re-purified using Ni-NTA-agarose beads. To generate higher protein concentrations, Fn-N10 and Fn-N17 were subcloned to create C-terminal maltose-binding protein fusions as described previously and purified by affinity chromatography (17). Binding reactions were carried out at room temperature for 30 min in 1× phosphate-buffered saline. Samples contained combinations of RNA, N, and 10Fn3 proteins at concentrations of 400 nM and 3.2 and 16 μM, respectively. 1.7 μl of 50% glycerol was added to 15-μl samples, which were separated on a 0.8% agarose gel stained with ethidium bromide.

RESULTS

mRNA Display Selection—We expressed and purified N protein from eukaryotic cells to retain native phosphorylation. The recombinant N protein was engineered with an N-terminal His_6 tag and an N-terminal biotinylation signal peptide for *in vitro* biotinylation. The specific biotinylation scheme allows

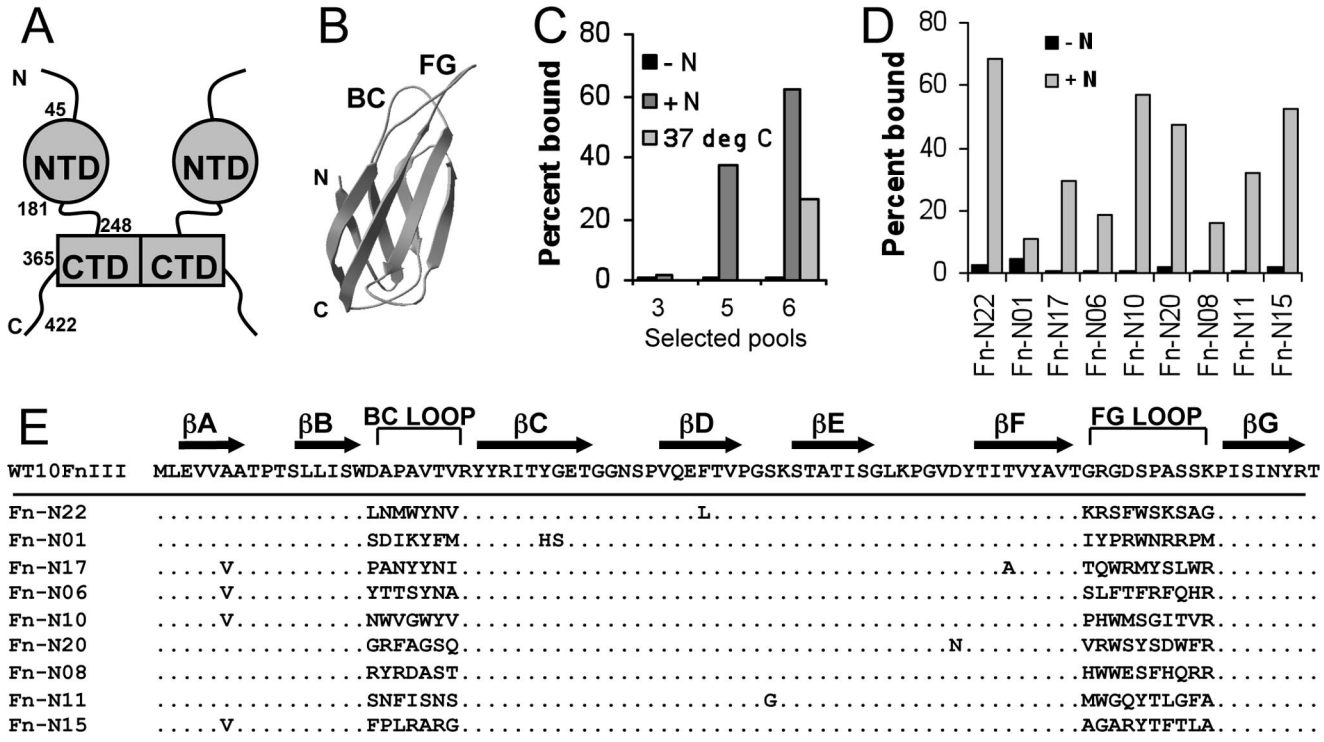

FIGURE 1. **mRNA display selection of 10Fn3 binders to N.** *A,* representative diagram of dimerized N protein. *B,* 10Fn3 domain. Seventeen residues in the BC and FG loops are randomized in our trillion member combinatorial library. *C,* radiolabeled *in vitro* binding assay for monitoring binder enrichment in selection pool 3, 5, and 6. The data are represented as the percentage of radioactive 10Fn3 proteins bound to the beads with N protein (+N) or beads only (−*N*). The pulldown assays were performed at 4 °C. Pool 6 binding was also performed at 37 °C. *D,* radiolabeled *in vitro* binding assay for individual binders. 9 representative binders were chosen from pool 6 for the pulldown assay as described in *C*. *E,* sequence alignment of the nine chosen binders.

directional immobilization via a specific lysine near the N terminus. We confirmed the functionality of the immobilized N protein by its ability to pull down free N protein and M protein.

For the selection of binders to N protein, we used the 10Fn3 scaffold library described previously by Olson and Roberts (15) (Fig. 1*B*). Our library began with a complexity of more than 1 trillion unique sequences, each present with ~10 copies. In each round, the cDNA/mRNA-protein library was incubated with immobilized N and washed, and the beads were amplified via PCR (see "Experimental Procedures"). Enrichment of target-specific binders was monitored by performing a radiolabeled pulldown assay for each round (Fig. 1*C*). After observing target-specific enrichment in pool 5, the stringency of the selection was increased by performing round 6 binding and washing at 37 °C. Pool 6 binding is very efficient with greater than 60% of the pool remaining bound at 4 °C and 30% at 37 °C.

Pool 6 was cloned, and 18 sequences were obtained (Fig. 1*E* and supplemental material). Of the 18 sequences, Fn-N22 was the most abundant with a total of six clones. The other sequences were represented by one (Fn-N01, Fn-N17, Fn-N08, Fn-N11, and Fn-N15) or two clones (Fn-N06, Fn-N10, and Fn-N20). Fn-N15 appeared nonspecific based on the presence of three arginine and two lysine residues in the BC loop and was not characterized further. The nine representative 10Fn3 proteins were each characterized for function, and all showed a better binding matrix bearing target than the matrix alone (Fig. 1*D*).

Notably, each of the nine N-binding 10Fn3 proteins tested had highly dissimilar sequences, arguing that each of these molecules recognizes N in a unique manner (Fig. 1, *D* and *E*). As expected, the binding analysis demonstrated that Fn-N22 has the best pulldown efficiency (68%), with little background binding. In rank order, the binding of the other clones followed Fn-N10 > Fn-N15 > Fn-N20 > Fn-N11 > Fn-N17. Fn-N06 and Fn-N08 had lower binding efficiency, whereas Fn-N01 had a relatively high background to target binding ratio and was not characterized further.

Expression and Binding Validation—We next sought to investigate the expression properties of the eight functional 10Fn3 variants (Fig. 2*A*). To do this, the 10Fn3 proteins were expressed in bacteria (Fig. 2*A*, *bottom panel*) and used to pull down FLAG-tagged N protein (Fig. 2*A*, *upper panel*). Although expression levels varied greatly, all eight 10Fn3 proteins were able to pull down the N protein, with Fn-N10 and Fn-N22 being most efficient (Fig. 2*A*). We next tested expression and binding of the selected 10Fn3 proteins in eukaryotic cells (293T cells, Fig. 2*B*). All eight of the 10Fn3 intrabodies (Fig. 2*B*, *top panel*) are able to co-express in these cells with N protein (Fig. 2*B*, *2nd panel*). FLAG-based immunoprecipitation of the 10Fn3 proteins is efficient (Fig. 2*B*, *3rd panel*), and three of the 10Fn3s demonstrated efficient co-immunoprecipitation of the N protein (Fn-N10, Fn-N17, and Fn-N20) (Fig. 2*B*, *bottom panel*). Using enzyme-linked immunosorbent assay, Fn-N17 and Fn-N20 were also demonstrated to function as well or better when compared with a high affinity anti-N monoclonal antibody (supplemental Fig. S1).

We next explored which regions of N were bound by the eight functional 10Fn3 domains. To do this, the full-length N

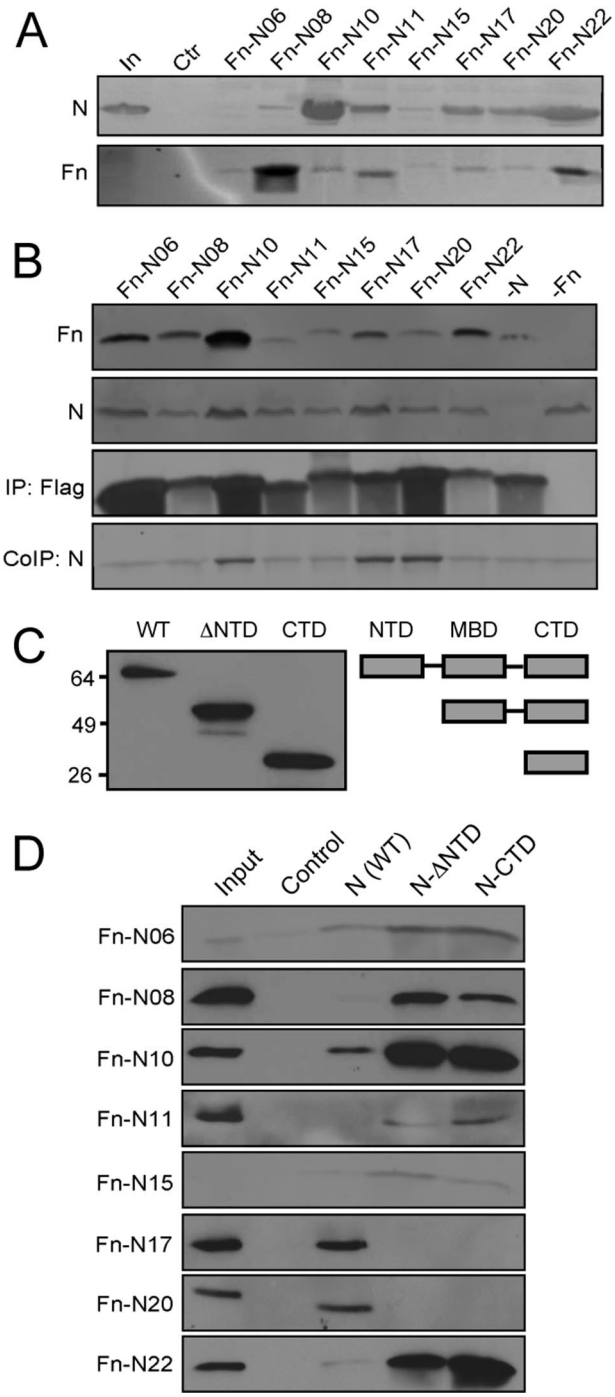

FIGURE 2. **Expression and binding of selected 10Fn3 proteins.** *A,* N protein pulldown by bacteria-derived 10Fn3 proteins. Ni-NTA bead-conjugated binders were used to pull down mammalian N protein from transfected cell lysates. The pulldown was analyzed by Western blot using antibody against FLAG tag for N and antibody against His_6 tag for 10Fn3 proteins. *In*, 2.5% of input lysate; *Ctr*, pulldown control using unconjugated Ni-NTA beads. *B,* co-immunoprecipitation (*CoIP*) of N protein with 10Fn3 proteins. 4% of input lysate was analyzed by Western blot using antibody against N and antibody against FLAG for 10Fn3 proteins. *9th lane* is Fn-N17 transfection only control. *10th lane* is N protein transfection only control. *C,* expression of full-length N protein and truncated mutants. The *left panel* is a Western blot analysis using anti His_6 tag antibody. The domain diagram on the *right* depicts the region of truncation. *WT*, full length; *ΔNTD*, N-terminal domain deletion mutant; *CTD*, C-terminal domain; *MBD*, M protein binding domain. *D,* domain specificity of N-binding 10Fn3 proteins. Immobilized His_6-tagged N-WT, ΔNTD, and CTD were used to pull down 10Fn3 proteins from 293T cell lysate. The pulldowns were analyzed by Western blot using antibody against FLAG-tag for 10Fn3 proteins. *Input*, 4% of input lysate; *Control,* unconjugated Ni-NTA beads control.

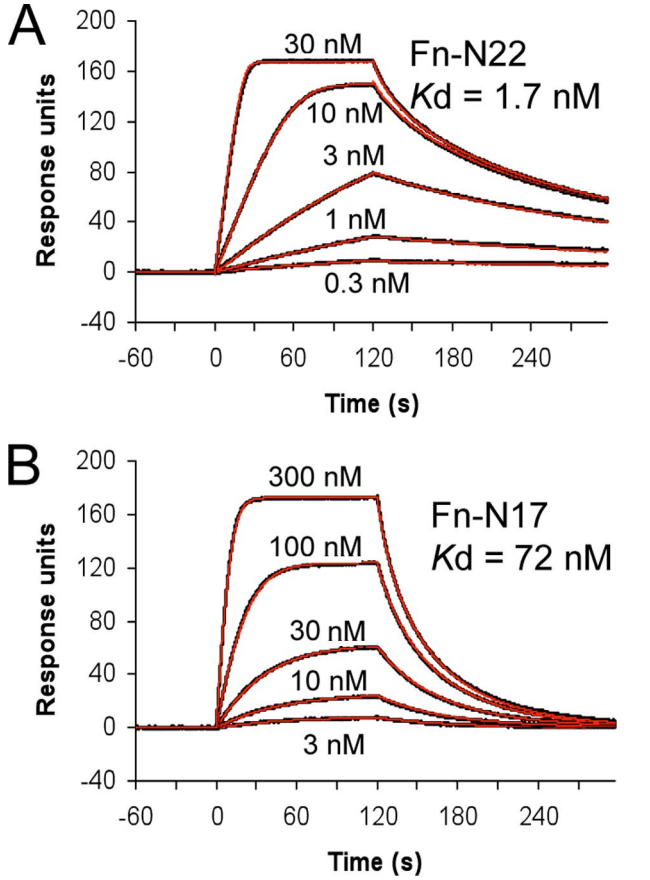

FIGURE 3. **Affinity of Fn-N17 and Fn-N22 for SARS N, determined by surface plasmon resonance.** Raw data are presented in *black*; *red* is the fitted curve.

(WT; residues 1–422), an N-terminal deletion mutant (ΔNTD; residues 182–422), and a C-terminal domain fragment (CTD; residues 248–422) were purified from 293T cells (Fig. 2*C*) and immobilized on nickel beads. The selected 10Fn3 proteins were expressed in mammalian cells with a C-terminal FLAG epitope for detection. Of the eight 10Fn3 proteins tested, Fn-N17 and Fn-N20 are pulled down only by the full-length N protein. Therefore, interaction with the N-terminal RNA binding domain is required for binding by Fn-N17 and Fn-N20 (Fig. 2*D*). The other six N-binders could be pulled down by all three N protein variants, indicating that they bind to the C-terminal self-association domain. It is interesting to note that the pulldown of all six CTD-specific binders was more efficient with constructs lacking the NTD.

Binding Affinity—We chose Fn-N22, a CTD binder, and Fn-N17, an NTD-dependent binder, to test the binding affinities achieved with this selection using surface plasmon resonance (Fig. 3). The N protein was prepped and purified with N-terminal specific biotinylation, allowing for directional immobilization on a Biacore streptavidin chip. For Fn-N22, the selection winner, the association rate constant was 2.17×10^7 M^{-1} s^{-1}, and the dissociation rate constant was 0.037 s^{-1}, resulting in an equilibrium dissociation constant (K_d) of 1.7 nM. For Fn-N17, the association rate constant was 8.71×10^5 M^{-1} s^{-1}, and the dissociation rate constant was 0.062 s^{-1}, resulting in a $K_d = 72$ nM ($\chi^2 = 0.3$ response unit^2 for each fit). The relative affinities

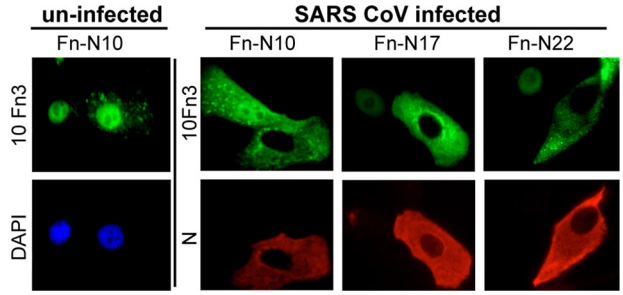

FIGURE 4. **Localization of 10Fn3 intrabodies in SARS-CoV-infected cells by immunofluorescence microscopy.** Fn-N10-, Fn-N17-, and Fn-N20-transfected VERO cells were either mock-infected or infected by SARS-CoV WT at a multiplicity of infection of 0.1 and were fixed at 16 h post-infection. 4′,6-Diamidino-2-phenylindole (*DAPI*) stains used for the nucleus. *Green,* 10Fn3; *red,* N protein.

were consistent with the relative *in vitro* pulldown efficiencies (68 *versus* 30%).

Cellular Localization—We next explored whether localization of the selected 10Fn3 intrabodies changes in response to the presence of N protein and whether these two proteins co-localize within mammalian cells (Fig. 4). To do this, we began by transfecting Fn-N10, Fn-N17, and Fn-N20 in VERO cells. In the absence of SARS N, each of these intrabodies shows substantial nuclear localization (Fn-N10 shown; Fig. 4), as shown by co-localization with 4′,6-diamidino-2-phenylindole stain, and gave diffuse fluorescence. Upon infection with SARS-CoV, the three intrabodies dramatically altered their localization, becoming cytosolic, and showed good overlap with SARS N localization. We also conducted similar experiments wherein the 10Fn3 intrabody and SARS N protein were both transfected into cells. Similarly, in these experiments we also observed movement of the intrabody to the cytosol and co-localization with SARS N (data not shown).

Inhibition of Viral Production—We next sought to test whether any of our selected 10Fn3 intrabodies affected viral production because of their interactions with SARS N. Formally, overexpression of our intrabodies could block virus production by a specific mechanism (*e.g.* direct interaction with N that alters some critical function) or by a nonspecific mechanism (*e.g.* by generically impairing general cellular functions). We began by measuring viral production with a variant of SARS-CoV bearing the *Renilla* luciferase gene (RL) in open reading frame 7 (24). Importantly, with this SARS-CoV strain, virus titer directly correlates with luciferase activity and enables the measurement of relative virus quantity over a large dynamic range. We first collected supernatant from SARS-CoV/RL-infected cells that express 10Fn3 intrabodies. To determine the relative virus titer, this supernatant was then used to infect secondary reporter cells, which were assayed 16 h post-infection.

All seven of the tested 10Fn3 strains inhibit viral production using the luciferase SARS-CoV variant (Fig. 5*A*), ranging from 11-fold to more than 5900-fold. Indeed, both C-terminal domain binding clones (FnN17 and FnN20) and N-terminal domain binding clones (Fn-N06, Fn-N10, Fn-N11, FnN15, and Fn-N22) were capable of inhibiting SARS-CoV production. Furthermore, inhibition of viral production was demonstrated to be dose-dependent (supplemental Fig. S2). The viral inhibition does not appear to be a function of the 10Fn3 protein

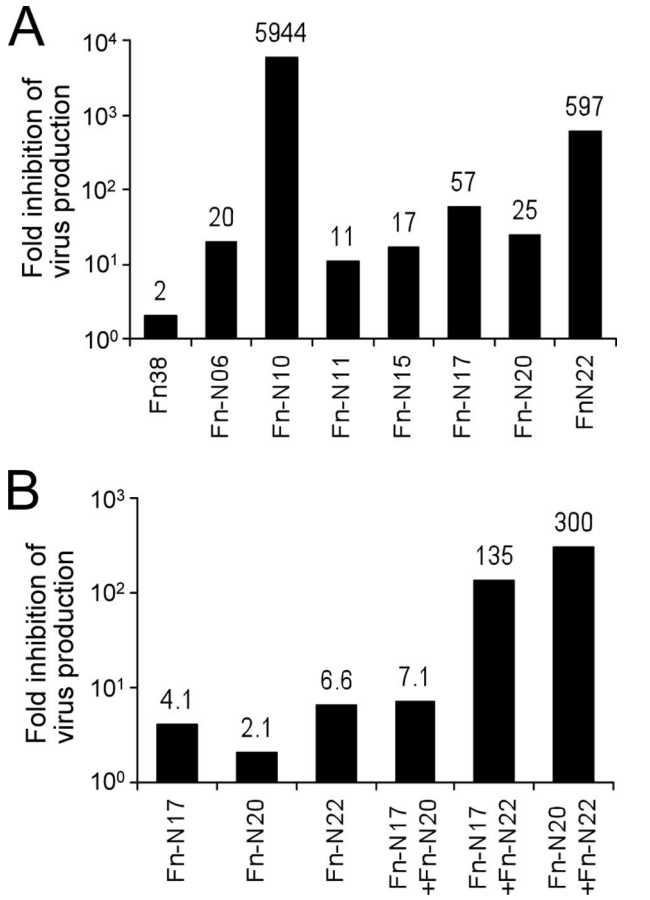

FIGURE 5. **Luciferase assay to determine inhibition of viral production.** 10Fn3 or mock-transfected 293T-Ace2 cells were infected at a multiplicity of infection of 0.5, and supernatants were collected 20 h post-infection. The cell supernatants were used to infect reporter cells to determine relative viral titers. Data are represented as the fold reduction in luciferase activity relative to control. *A,* 10Fn3 intrabodies inhibit viral production. *B,* cooperative inhibition by 10Fn3 intrabodies.

scaffold, as transfection and overexpression of Fn38 (a randomly chosen, nonfunctional clone characterized previously (15)) show a modest 2-fold decrease in virus production.

We next evaluated whether 10Fn3 intrabodies that recognize nonoverlapping epitopes could inhibit virus production synergistically. To test this, the two NTD-dependent binders (Fn-N17 and Fn-N20) and the highest affinity CTD binder (Fn-N22) were co-transfected into cells (Fig. 5*B*). These experiments were done at lower DNA concentration than the single fibronectin experiments (Fig. 5*A*) to enable us to accurately demonstrate the synergistic inhibition generated by two potent inhibitors. At this concentration, expression of Fn-N17, Fn-N20, and Fn-N22 alone inhibits viral production 4-, 2-, and 6.6-fold, respectively. Co-expression of the two NTD binders (Fn-N17 and Fn-N20) together had an additive effect on virus inhibition (7.1-fold), consistent with simply increasing the inhibitory intrabody concentration. Interestingly, co-expression of Fn-N17 with Fn-N22 or Fn-N20 with Fn-N22 resulted in 135–300-fold inhibition, consistent with both combinations of 10Fn3 intrabodies recognizing unique sites simultaneously and exerting cooperative inhibition of SARS-CoV production.

Inhibition of SARS-CoV Gene Expression—Our virus production assays involve two steps (Fig. 5) and are able to detect even

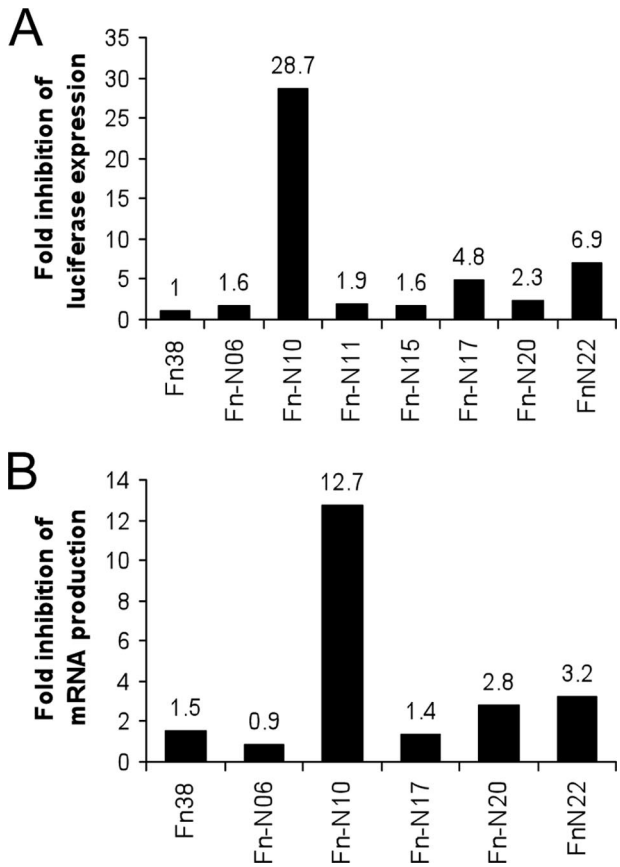

FIGURE 6. **10Fn3 intrabodies inhibit viral gene expression.** *A,* 10Fn3 intrabodies inhibit luciferase expression. 293T-Ace2 cells were transfected with each 10Fn3 intrabody and infected with SARS-CoV/RL virus at multiplicity of infection 0.5. *Renilla* luciferase activities were assayed at 20 h post-infection. The fold inhibition of luciferase expression is defined as the ratio of luciferase activity from cells transfected with empty plasmid relative to cells transfected with 10Fn3 intrabodies. *B,* 10Fn3 intrabodies inhibit viral gene transcription. Quantitative PCR was performed using SARS-CoV N mRNA. The amount of N transcript was normalized to actin transcript control. Data are represented as fold reduction of calculated copy number.

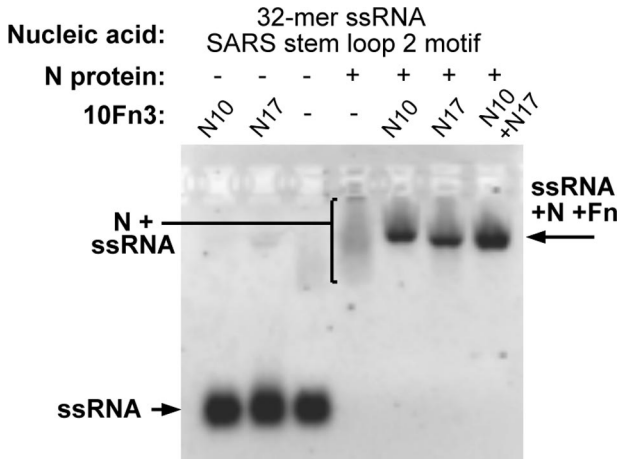

FIGURE 7. **Effect of 10Fn3 inhibitors on N binding to RNA.** The binding reactions contain mixtures of s2m RNA (0.4 μM), nuclease-treated N (3.2 μM), and 10Fn3-maltose-binding protein fusions (16 μM). *3rd lane* includes 1 μg of bovine serum albumin. Binding reactions were run on a 0.8% agarose gel and stained with ethidium bromide.

very small amounts of virus. On the other hand, they are an indirect measure of virus replication, as the virus is propagated in the second step. We sought to directly measure the ability of the 10Fn3 intrabodies to inhibit gene expression in the original infected cells (Fig. 6). We did this in two ways. First, we monitored the inhibition of luciferase production directly using SARS-CoV/RL in 293T-Ace cells (Fig. 6*A*). Second, we directly measured mRNA production using quantitative reverse transcription-PCR with wild type SARS-CoV in the same cell line (Fig. 6*B*).

Both experiments show that NTD- and CTD-binding 10Fn3s inhibit gene expression directly (Fig. 6, *A* and *B*). Looking at luciferase production (Fig. 6*A*), Fn-N17, Fn-N22, and Fn-N10 give the best inhibition, ranging from 4.8- to 29-fold compared with the no fibronectin control. Fn-N11, Fn-N15, and Fn-N20 gave reduced but measurable inhibition, ranging from 1.6- to 2.3-fold. Importantly, the nonfunctional clone, Fn38, gave no inhibition, indicating that expression of an exogenous fibronectin has little effect on our assay. We note that four inhibitors tested (Fn-N10, Fn-N17, Fn-N20, and Fn-N22) displayed inhibition in a dose-dependent manner (supplemental Fig. S3).

We next used quantitative reverse transcription-PCR to measure the effect of our selected 10Fn3s on viral mRNA levels (specifically, the subgenomic mRNA; Fig. 6*B*). Similar to the luciferase assay, the best inhibitors were Fn-N20, Fn-N22, and Fn-N10, which decrease viral mRNA levels from 2.8- to ~13-fold. Fn-N17 and Fn-N06 showed less inhibition than the Fn38, the nonfunctional control. Northern blot analysis confirmed that other SARS transcripts were reduced in the same trend as the open reading frame N subgenomic mRNA (data not shown). Furthermore, Western blot analysis demonstrated that Fn-N22, Fn-N10, Fn-17, and (to a lesser extent) Fn-N20 prevent accumulation of SARS structural proteins (supplemental Fig. S4).

Finally, we wished to demonstrate that the inhibition we observed was specific to the SARS virus. For example, if the selected 10Fn3s aggregated or misfolded, they might generally disrupt cellular function, thereby inhibiting virus production. To address this, we transfected each of our 10Fn3s into cells and then performed a luciferase-based inhibition assay with the herpesvirus variant MHV-68/M3Luc. In these experiments, only one of our eight selected binders (Fn-N08) inhibited MHV-68/M3Luc expression (data not shown). Thus, we did not include Fn-N08 in our inhibition or co-localization studies (Figs. 4–6). We also demonstrated that the best inhibitors (Fn-N10, Fn-N22, Fn-N17, and Fn-N20) do not effect MHV-68 capsid protein expression (supplemental Fig. S5).

Effect of 10Fn3 Proteins on RNA Binding—N protein normally exists as a dimer and is capable of binding and band-shifting SARS RNA. To conclude this work, we sought to determine the effect of our selected 10Fn3 proteins on N protein RNA binding as measured by band shifts. To do this, we used a 32-mer single-stranded RNA segment of the SARS stem loop 2 motif (s2m) previously used by Chen *et al.* (28). Fig. 7 demonstrates that Fn-N10 and Fn-N17 do not inhibit N binding to SARS s2m RNA. However, both the CTD binding Fn-N10 and the NTD-dependent binder Fn-N17 have the effect of resolving the diffuse, low mobility N-RNA complex to a well defined band. This indicates that the 10Fn3 proteins are able to bind the

N-RNA complex, forming a ternary complex. The nature of this ternary complex is not clear. N protein exists as a dimer in solution and is able to form larger oligomeric states at higher concentrations and in the presence of nucleic acid (28–30). The diffuse N-RNA band may be due to the presence of multiple oligomerization states, whereas the resolving effect of the 10Fn3 inhibitors may be indicative of either a single conformation state or a soluble, high molecular weight complex of N protein, s2m RNA, and 10Fn3.

DISCUSSION

Our data demonstrate that directed evolution by mRNA display enabled designing of at least eight novel high affinity protein reagents targeting the SARS nucleocapsid protein (Fig. 1, *D* and *E*; Fn-N22, Fn-N17, Fn-N06, Fn-N06, Fn-N20, Fn-N08, Fn-N11, and Fn-N15). The pool showed a high fraction of binding (~25%) even at physiologic temperature and salt. Biochemically, the best binder, Fn-N22, was the most abundant member of the cloned sequences (6 of 18 cloned) indicating that the pool was converging to a selection winner. None of the distinct clones are related by homology, indicating each is an independent solution to the binding problem we presented the library. Each of the loop sequences contains a high representation of aromatic and polar residues, typical of protein interaction surfaces (31). Given the relatively small number of pool members sequenced (18 total), it is likely that there are many more than eight independent binders in our round 6 pool.

The selected 10Fn3 proteins were functional, well behaved, and able to be expressed in a number of formats. In addition to the reticulocyte lysate expression system used for library construction, 10Fn3 proteins were expressed in bacteria and mammalian cells, including 293T and VERO cells (Figs. 2–6).

Interestingly, our selection revealed two distinct binding sites on N for 10Fn3 recognition, the NTD and CTD (Fig. 1*A*). Six of the eight 10Fn3s bind the CTD alone (Fn-N06, Fn-N08, Fn-N10, Fn-N11, Fn-N15, and Fn-N22), whereas the other two (Fn-N17 and Fn-N20) require the NTD to bind. Structurally, the NTD and CTD are connected by unstructured regions (see Fig. 1*A*, *schematic*) and have been reported to be noninteracting (32). On the other hand, three of our CTD binders (Fn-N08, Fn-N10, and Fn-N22) show markedly improved binding to N constructs lacking the N-terminal domain (Fig. 2*D*), indicating the NTD may partially occlude the binding site on the CTD.

One CTD binder (Fn-N22) and one NTD-dependent binder (Fn-N17) were analyzed for affinity. The monovalent Fn-N22 and Fn-N17 bind to N protein with high affinity, similar to or better than the larger Fv region of monoclonal antibodies (K_d = 1.7 and 72 nM, respectively) (33). Even though this affinity is high, it is likely that affinity maturation and evolution could improve these affinities further, opening the potential that these binders could be used in ultra-sensitive detection platforms.

A remarkable aspect of our work is that at least four of the selected 10Fn3 proteins (Fn-N10, Fn-N17, Fn-N20, and Fn-N22) specifically and dramatically inhibit SARS-CoV replication when transiently expressed in mammalian cell culture. Several points are worth noting. Generally, overexpression of the 10Fn3s is well tolerated inside the cell lines tested. 10Fn3 expression is relatively diffuse, with a higher density in the nucleus. Also, the 10Fn3 proteins are re-localized to the cytoplasm by N, demonstrating the potential for these molecules as tools for real time visualization (Fig. 4). Finally, the majority of the selected 10Fn3s (7/8 functional proteins) do not inhibit cellular function as measured in a relatively stringent assay, the ability to propagate an unrelated virus, herpesvirus.

Functionally, ligands targeting the CTD (Fn-N10 and Fn-N22) appear to have a larger inhibitory effect compared with the NTD-dependent binders. Furthermore, combining an NTD and CTD binder results in synergistic inhibition (Fig. 5*B*). Our findings are reminiscent of the common antiviral mixture therapeutic strategy. Our findings are reminiscent of common antiviral mixture therapeutic strategies, where multiple small molecules drugs are used to target two or more key viral enzymatic functions. Here we have demonstrated that targeting two distinct protein surfaces of the nonenzymatic nucleocapsid protein also provides cooperative inhibition of virus production, a novel and intriguing result.

Finally, we sought to characterize how our selected 10Fn3s might affect N function. The NTD of N is thought to mediate binding to the genomic RNA essential for the formation of ribonucleoprotein complex (20). To determine whether 10Fn3 intrabodies inhibit SARS replication by effecting nucleic acid binding, we tested RNA band shifts using a portion of the SARS s2m. Both Fn-N10, the best inhibitor and a CTD binder, and Fn-N17, an NTD-dependent binder, do not compete with the RNA for binding to N. Both molecules have the effect of resolving the band formed by the complex. Although the band shift is well resolved, its low mobility makes it difficult to conclusively determine the effect of 10Fn3s on N oligomerization. Based on the data, our working hypothesis is that the 10Fn3 proteins reduce the structural and oligomeric heterogeneity of the N-RNA complexes.

This study demonstrates the utility of using mRNA display selections to generate selective, high affinity 10Fn3-based proteins that target specific cellular components. 10Fn3 intrabodies are able to be expressed in bacteria for biophysical characterization and are stable in mammalian cells, advantages over the commonly used antibody scaffold. Importantly, no *in vivo* screen was required to filter the resulting pool for binders that function inside the cell. Of the eight intrabodies tested, seven function efficiently to block SARS replication and do not disrupt mammalian cellular function (Fig. 2*B*).

Used inside cells, 10Fn3s provide a complementary tool to commonly used methods for the analysis of proteins *in vivo* such as gene knock-outs and small interfering RNA. The N binders described in this study may thus be useful for future studies of SARS virus. For example, N binders may shed light on key N protein-host cell protein interactions during various stages of the virus life cycle. Our results demonstrate that 10Fn3 intrabodies enable *in vivo* visualization of N. Therefore, the 10Fn3s may enable analyzing the fate of N and the ribonucleoprotein complex in real time during the various stages of the virus life cycle. This would be especially useful during the initial stages of virus entry, where reverse genetics cannot be easily applied because infectious viral particles may not be generated without functional viral capsid or envelope proteins. Finally,

the biological neutrality of the 10Fn3s implies that combining two or more inhibitors may be useful clinically as an approach toward improving gene therapy-based preventative interventions for persistent viral diseases.

Acknowledgment—We thank the University of Southern California Nanobiophysics core facility for Biacore use.

REFERENCES

1. Maynard, J., and Georgiou, G. (2000) *Annu. Rev. Biomed. Eng.* **2,** 339–376
2. Lipovsek, D., and Plückthun, A. (2004) *J. Immunol. Methods* **290,** 51–67
3. Hosse, R. J., Rothe, A., and Power, B. E. (2006) *Protein Sci.* **15,** 14–27
4. Roberts, R. W., and Szostak, J. W. (1997) *Proc. Natl. Acad. Sci. U. S. A.* **94,** 12297–12302
5. Carlson, J. R. (1988) *Mol. Cell. Biol.* **8,** 2638–2646
6. Stocks, M. (2005) *Curr. Opin. Chem. Biol.* **9,** 359–365
7. Nizak, C., Monier, S., del Nery, E., Moutel, S., Goud, B., and Perez, F. (2003) *Science* **300,** 984–987
8. Rajpal, A., and Turi, T. G. (2001) *J. Biol. Chem.* **276,** 33139–33146
9. Visintin, M., Tse, E., Axelson, H., Rabbitts, T. H., and Cattaneo, A. (1999) *Proc. Natl. Acad. Sci. U. S. A.* **96,** 11723–11728
10. Vascotto, F., Campagna, M., Visintin, M., Cattaneo, A., and Burrone, O. R. (2004) *J. Gen. Virol.* **85,** 3285–3290
11. Cardinale, A., Filesi, I., Mattei, S., and Biocca, S. (2003) *Eur. J. Biochem.* **270,** 3389–3397
12. Cardinale, A., Filesi, I., and Biocca, S. (2001) *Eur. J. Biochem.* **268,** 268–277
13. Kawe, M., Forrer, P., Amstutz, P., and Plückthun, A. (2006) *J. Biol. Chem.* **281,** 40252–40263
14. Amstutz, P., Binz, H. K., Parizek, P., Stumpp, M. T., Kohl, A., Grütter, M. G., Forrer, P., and Plückthun, A. (2005) *J. Biol. Chem.* **280,** 24715–24722
15. Olson, C. A., and Roberts, R. W. (2007) *Protein Sci.* **16,** 476–484
16. Koide, A., Bailey, C. W., Huang, X., and Koide, S. (1998) *J. Mol. Biol.* **284,** 1141–1151
17. Olson, C. A., Liao, H. I., Sun, R., and Roberts, R. W. (2008) *ACS Chem. Biol.* **3,** 480–485
18. Rota, P. A., Oberste, M. S., Monroe, S. S., Nix, W. A., Campagnoli, R., Icenogle, J. P., Peñaranda, S., Bankamp, B., Maher, K., Chen, M. H., Tong, S., Tamin, A., Lowe, L., Frace, M., DeRisi, J. L., Chen, Q., Wang, D., Erdman, D. D., Peret, T. C., Burns, C., Ksiazek, T. G., Rollin, P. E., Sanchez, A., Liffick, S., Holloway, B., Limor, J., McCaustland, K., Olsen-Rasmussen, M., Fouchier, R., Günther, S., Osterhaus, A. D., Drosten, C., Pallansch, M. A., Anderson, L. J., and Bellini, W. J. (2003) *Science* **300,** 1394–1399
19. Surjit, M., Liu, B., Kumar, P., Chow, V. T., and Lal, S. K. (2004) *Biochem. Biophys. Res. Commun.* **317,** 1030–1036
20. Saikatendu, K. S., Joseph, J. S., Subramanian, V., Neuman, B. W., Buchmeier, M. J., Stevens, R. C., and Kuhn, P. (2007) *J. Virol.* **81,** 3913–3921
21. Satija, N., and Lal, S. K. (2007) *Ann. N.Y. Acad. Sci.* **1102,** 26–38
22. Enjuanes, L., Almazán, F., Sola, I., and Zuñiga, S. (2006) *Annu. Rev. Microbiol.* **60,** 211–230
23. Yount, B., Curtis, K. M., Fritz, E. A., Hensley, L. E., Jahrling, P. B., Prentice, E., Denison, M. R., Geisbert, T. W., and Baric, R. S. (2003) *Proc. Natl. Acad. Sci. U. S. A.* **100,** 12995–13000
24. Roberts, R. S., Yount, B. L., Sims, A. C., Baker, S., and Baric, R. S. (2006) *Adv. Exp. Med. Biol.* **581,** 597–600
25. Ja, W. W., Adhikari, A., Austin, R. J., Sprang, S. R., and Roberts, R. W. (2005) *J. Biol. Chem.* **280,** 32057–32060
26. Liu, R., Barrick, J. E., Szostak, J. W., and Roberts, R. W. (2000) *Methods Enzymol.* **318,** 268–293
27. Milligan, J. F., Groebe, D. R., Witherell, G. W., and Uhlenbeck, O. C. (1987) *Nucleic Acids Res.* **15,** 8783–8798
28. Chen, C. Y., Chang, C. K., Chang, Y. W., Sue, S. C., Bai, H. I., Riang, L., Hsiao, C. D., and Huang, T. H. (2007) *J. Mol. Biol.* **368,** 1075–1086
29. Luo, H., Chen, J., Chen, K., Shen, X., and Jiang, H. (2006) *Biochemistry* **45,** 11827–11835
30. Yu, I. M., Gustafson, C. L., Diao, J., Burgner, J. W., 2nd, Li, Z., Zhang, J., and Chen, J. (2005) *J. Biol. Chem.* **280,** 23280–23286
31. Chakrabarti, P., and Janin, J. (2002) *Proteins* **47,** 334–343
32. Chang, C. K., Sue, S. C., Yu, T. H., Hsieh, C. M., Tsai, C. K., Chiang, Y. C., Lee, S. J., Hsiao, H. H., Wu, W. J., Chang, W. L., Lin, C. H., and Huang, T. H. (2006) *J. Biomed. Sci.* **13,** 59–72
33. Carter, P. J. (2006) *Nat. Rev. Immunol.* **6,** 343–357